RSC Advances

PAPER

View Article Online
View Journal | View Issue

Cite this: *RSC Adv.*, 2020, **10**, 53

Photocatalytic coatings based on a zinc(II) phthalocyanine derivative immobilized on nanoporous gold leafs with various pore sizes†

David Steinebrunner,[ab] Günter Schnurpfeil,[c] Dieter Wöhrle*[c] and Arne Wittstock*[ab]

A series of singlet oxygen sensitizing hybrid materials is reported consisting of a zinc(II) phthalocyanine (ZnPc) derivative immobilized on nanoporous gold leafs (npAu) with various pore sizes. The resulting photocatalytic coatings exhibit a thickness of around 100 nm and pore sizes between 9–50 nm. Herein, we report the synthesis and characterization of those hybrid materials which were synthesized by functionalization of npAu leafs by an azide terminated alkanethiol self-assembled monolayer (SAM) and subsequent copper catalyzed azide–alkyne cycloaddition (CuAAC). The characterization of the samples morphology included scanning electron microscopy (SEM), UV-Vis spectroscopy as well as energy dispersive X-ray spectroscopy (EDX). The morphology–reactivity relationship was investigated employing the hybrid photocatalysts in the photooxidation of diphenylisobenzofuran (DPBF) as selective singlet oxygen quencher. An increasing photocatalytic activity was found for smaller pore sizes up to 15 nm, due to the gain in specific surface area concomitant with an increasing amount of immobilized photosensitizer, completely dominating the effect of the higher spectral overlap caused by the shift of the plasmon resonance of npAu, until mass transport and diffusion limitation gets predominant for pore sizes below 15 nm.

Received 28th October 2019
Accepted 16th December 2019

DOI: 10.1039/c9ra08841e

rsc.li/rsc-advances

Introduction

Porous materials have gained growing attention during the last decades in many different fields such as catalysis, sensor applications or electrode materials due to the high specific surface area arising from its porosity and small size feature.[1–11] In addition, the formation of nanoporosity leads to new active materials as it was shown in the case of npAu.[12–14] While gold as bulk material is relatively inactive in chemical reactions, npAu was shown to be a very efficient catalyst for several oxidation reactions in both, gas phase and liquid phase even at comparably low temperatures.[15–18] Besides this, the formation of porosity in the nanometer scale is also the reason for arising special optical features such as surface plasmon resonance similar to gold nanoparticles (AuNPs).[19–21] Using surface gold chemistry, which is well established in literature, the nanoporous material can be easily functionalized in many ways, for example with different metal oxide nanoparticles as well as several organometallic complexes or even proteins using the principles of self-assembled monolayers.[1,22–25] The introduction of light absorbing chromophores is thereby of great interest, as interactions with the surface plasmons of gold nanostructures were shown to have an increasing effect onto the photocatalytic activity of such hybrid materials.[26–30] Recent studies revealed an increase in singlet oxygen formation by nearly an order of magnitude when a zinc(II) phthalocyanine derivative was immobilized onto a npAu as additional chromophore, that can be used for example for the photooxidation of citronellol, a reaction that is also of industrial relevance.[24] A severe drawback in heterogeneous photocatalysis with porous catalysts is the limited penetration depth of visible light in such materials. In the case of npAu it was shown by UV-Vis spectroscopy in transmission mode that the penetration maximum is around 300 nm, and therefore in conventional npAu catalysts a high amount of the noble and expensive gold materials is inactive in the dark zone.[25] To overcome this problem the usage of a thin film npAu support is beneficial. Such npAu films were first reported by J. Erlebacher and coworkers in 2004 who showed that such films with a thickness of around 100 nm can be easily prepared by floating white gold leaf (Ag/Au alloy) on concentrated nitric acid.[31] Using this approach, monolithic npAu films with various pore sizes can be obtained by adjusting the employed dealloying time of the precursor alloy foil. The

[a]*Institute of Applied and Physical Chemistry and Center for Environmental Research and Sustainable Technology, University Bremen, Leobener Str. UFT, 28359 Bremen, Germany. E-mail: awittstock@uni-bremen.de*

[b]*MAPEX Center for Materials and Processes, University Bremen, Bibliothekstr. 1, 28359 Bremen, Germany*

[c]*Organic and Macromolecular Chemistry, University Bremen, Leobener Str. NW2, 28359 Bremen, Germany. E-mail: woehrle@uni-bremen.de*

† Electronic supplementary information (ESI) available. See DOI: 10.1039/c9ra08841e

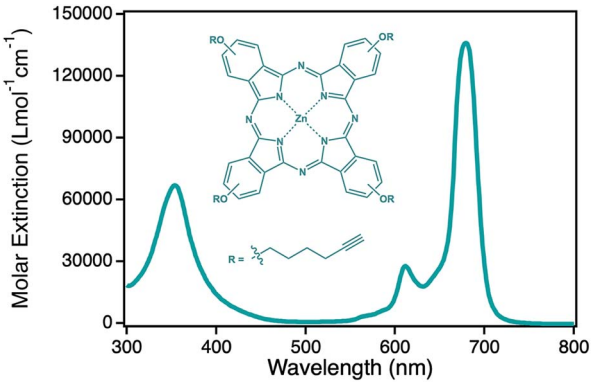

Fig. 1 Structure and corresponding optical spectrum of the photosensitizer zinc(II) phthalocyanine **2** used in this study.

variation of the pore sizes is coherent with a shift of the plasmonic peak, where the longitudinal part shifts from around 550 nm at small pores below 10 nm up to 650 nm for pores around 50 nm.[19,20] The transversal part of the signal on the other hand stayed constant at around 490 nm.[21] In this study we used a npAu coating material prepared from cheap, commercial gold foils which were functionalized *via* the established two step synthesis approach with a ZnPc derivative (Fig. 1) as first time reported hybrid material consisting of a macrocyclic metal complex immobilized on a npAu foil.[24,25] In our preliminary work we have shown that the immobilization of such a chromophore onto npAu disks and powders results in a significant increase in photocatalytic singlet oxygen production by nearly an order of magnitude due to a synergistic effect between the plasmon resonance of the npAu support and the immobilized photosensitizer.[25] The aim of the present study is to investigate in detail the effect of the pore size on such hybrid systems. As mentioned beforehand, the variation of the pore size induces a shift of the plasmonic signal, resulting in a higher spectral overlap integral for larger pore sizes, which should have an impact on the energy transfer rate to the sensitizer.[32–34] In contrast, a variation of the pore size also changes the available specific surface area and will lead to a higher amount of immobilized sensitizer for samples with smaller pores. Finally, the question of mass transport and diffusion limitation will be investigated for samples with small pore sizes to determine the ideal pore size for the hybrid photocatalyst where the interplay between the three opposing factors mentioned beforehand will result in the highest singlet oxygen sensitization activity.

Experimental

Materials

Ag/Au foils were received from Noris Blattgold GmbH, Schwabach, Germany (American white gold, 12 karat, Ag : Au 50 : 50 wt%). *S*-(6-azidohexyl)ethanethioate (**1**), the co-catalyst tris(benzyltriazolylmethyl)amine (TBTA) and the photo-sensitizer 2,9,16,23-tetrakis(4-hex-5-yn-oxy)phthalocyanine-zinc(II) (**2**) were synthesized as described previously according to literature procedures.[24,25,35–39] Hydroquinone was obtained from Merck, $Cu(MeCN)_4PF_6$ (97%) from Aldrich and 1,3-diphenylisobenzofuran (DPBF (**3**), >95%) from TCI. Ethanol (abs., reagent grade), THF (reagent grade, ≥ 99.0%), DMF (analytical reagent grade, ≥ 99.5%) and HNO_3 (analytical reagent grade, 65 wt%) were all received from VWR and were used without further purification. UV-Vis spectra of ZnPc **2**, npAu and for the measurements of the photocatalytic oxidations were recorded on a UV-1600PC UV-Vis spectrometer from VWR.

Nanoporous gold (npAu) preparation

npAu foils with various pore sizes were prepared according to a literature procedure.[31] The starting Ag/Au alloy (12 karat white-gold leaf, 50 : 50 wt%, 100 nm thickness) was cut into pieces of 1.5 × 1.5 cm, transferred onto a microscope glass slide and dealloyed by floating on concentrated HNO_3 (50 mL, 65 wt%) for 15 min, 30 min, 2 h, 8 h or 72 h, respectively. After dealloying, the foil was washed by floating on deionized water for 30 min, transferred onto a microscope cover glass and dried at ambient atmosphere overnight. The pore and ligament sizes of the npAu foils were analyzed by scanning electron microscopy.

Hybrid preparation

The as prepared npAu foils were immersed into a solution of *S*-(6-azidohexyl)ethanethioate (**1**, 100.6 mg, 0.5 mmol) dissolved in EtOH (10 mL) for 24 h. Then the samples were repeatedly washed with EtOH to remove any physisorbed material.

The as prepared functionalized npAu samples bearing an azide terminated SAM were immersed into a solution of ZnPc (**2**, 144.2 μg, 0.15 μmol), $Cu(MeCN)_4PF_6$ (931.8 μg, 2.5 μmol), TBTA (1.326 mg, 2.5 μmol) and hydroquinone (272.5 μg, 2.5 μmol) in a THF/H_2O mixture (10 mL, 3 : 1 v%). After a reaction time of 72 h, the sample was repeatedly washed with THF to remove any unbound ZnPc.

Characterization methods

For determination of the pore and ligament sizes of the npAu supports as well as the zinc distribution the samples were transferred onto a microscope sample holder with a conductive carbon tape. Micrographs of the samples morphology were acquired with a Supra 40 (Zeiss, Germany) scanning electron microscope operated at 10.0 kV acceleration voltage, 300 pA probe current and 4 mm working distance. The pore and ligament sizes were determined by measuring the diameter of at least 250 pores or ligaments in the obtained SEM images using the program ImageJ. The specific surface area S was calculated from the ligament diameter d according to $S = (C/\rho d)$ where C is the porosity factor for npAu with 3.7 and ρ is the gold bulk density of 19.8 g cm^{-3} according to literature.[40,41] This method was shown to give values that are in good agreement with both, data from gas adsorption experiments (BET) as well as electrochemical methods (CV).[40,41] The amount of immobilized ZnPc as well as the zinc distribution on the surface were determined by energy dispersive X-ray spectroscopy (EDX, Bruker XFlash 6/30).

Photocatalytic oxidation

Photocatalytic oxidations were performed in a self-built reaction setup as described previously.[25] Irradiation was carried out using

a 300 W Xe-arc lamp (LOT qd GmbH, Darmstadt, Germany) equipped with a 550 nm cut-on filter from Andover to achieve simultaneous irradiation of the plasmon resonance of npAu between 550–650 nm and the Q-band of the immobilized ZnPc at 690 nm without decomposition of DPBF which would occur at wavelengths < 500 nm.

For each photocatalytic experiment the respective hybrid catalyst (1.5 × 1.5 cm, ~0.05 mg) supported on a microscope cover slide was fixed at the rear screwing facing the inside of the gas cuvette to achieve a reproductive fixation of the catalyst at the same position in the light beam and distance to the light source (Fig. S1†). Then the reactor was filled with DMF (100 mL) and stirred under oxygen atmosphere for 10 min to achieve gas saturation of the reaction solution. Subsequently DPBF (1.35 mg, 5 μmol) was added, the vessel closed with a septum and irradiation started. Samples were collected every 120 s *via* syringe and the DPBF concentration was measured using UV-Vis spectroscopy and calculated at the absorption maximum at 415 nm using Lambert Beers law and the extinction coefficient of ε_{415} = 23 000 L mol^{-1} cm^{-1}.[42]

Results and discussion

Preparation and characterization of npAu foils with various pore sizes

npAu samples bearing various pore sizes were obtained by dealloying commercial Ag/Au gold foils in concentrated HNO_3 employing different dealloying times. The interruption of the dealloying process by transferring the sample from the acid onto water immediately stops the process resulting in samples with pore sizes between 10 and 50 nm and a thickness of around 100 nm (Fig. S2†).[19,31] The morphology of the obtained samples was analyzed by SEM, which shows the expected trend in pore size ranging from 9.5 nm after a dealloying time of 15 min up to 48.5 nm after 72 h (Fig. 2). All samples show a Gaussian like distribution regarding the pore sizes, which broadens for samples with larger pores. The determined ligament sizes were similar in size to the pores, and only samples with larger pore sizes showed a significant deviation resulting in larger ligaments. The position of the LSPR band in npAu foils is known to be dependent on the pore size of the sample as well as the dielectric environment of the surrounding media.[19] As many photocatalytic experiments are performed in DMF, due to the high singlet oxygen lifetime in this solvent and reasonable oxygen solubility capacity, the position of the LSPR band of the npAu supports in a DMF environment was of major interest (Fig. 3).[43,44] For this, the samples were sandwiched between two microscope cover glasses and two drops of DMF added between them. Subsequently, the samples were placed inside a UV/Vis spectrometer and measured in transmission mode, measuring the extraordinary optical transmission (EOT) arising from the plasmon resonance of the npAu films. The obtained spectra showed two different plasmonic peaks for each npAu sample which are ascribed to the longitudinal and the transverse LSPR in the ligaments.[21] Whereas the two LSPR peaks could be resolved using DMF as surrounding environment, the

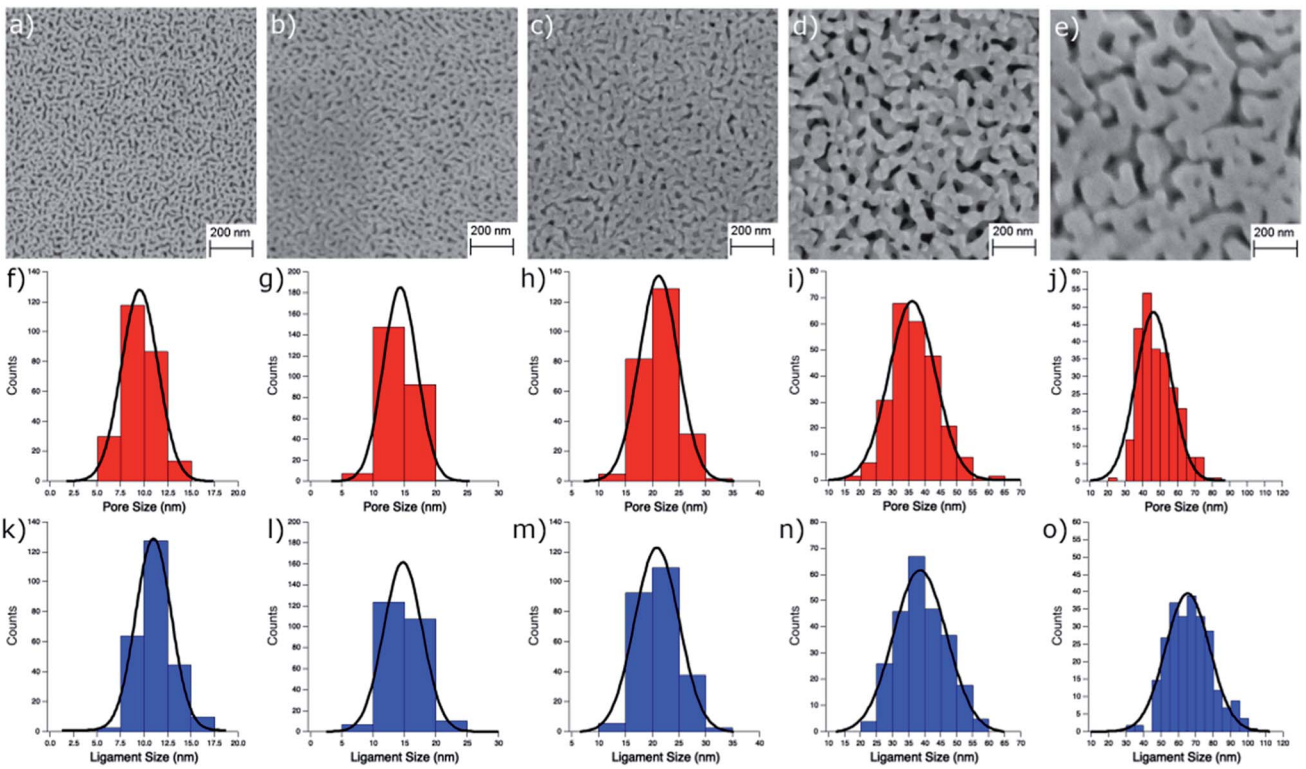

Fig. 2 SEM images of the structure of npAu foils after dealloying times of (a) 15 min, (b) 30 min, (c) 2 h, (d) 8 h and (e) 72 h. Distribution curves for the pore sizes (f–j) and for the ligament sizes (k–o) of the prepared npAu foils all show a Gaussian distribution and are used for the calculation of the specific surface area.

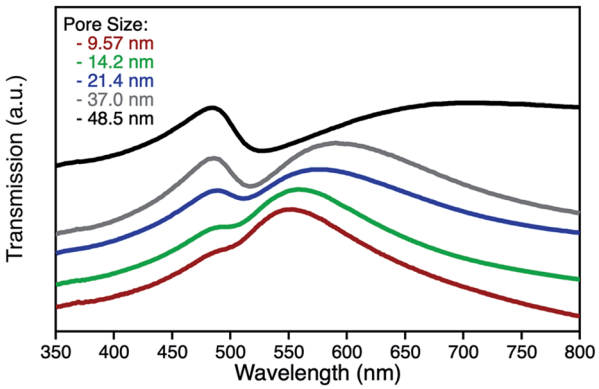

Fig. 3 UV-Vis transmission spectra of unfunctionalized npAu foils in a DMF surrounding environment after dealloying times of 15 min (red), 30 min (green), 2 h (blue), 8 h (grey) and 72 h (black).

measurements in air only gave an averaged signal where no shifting trends of the signals were observed. In contrast, a significant red-shift was observed for the long-wavelength peak with increasing pore size of the npAu, while the short-wavelength peak remains unchanged. Similar trends were shown providing other solvents like water, EtOH or toluene as surrounding dielectric environment to the npAu material.[19,21] The possibility to tune the position of the plasmonic absorption of the npAu supports might be a promising strategy to enhance energy transfer in hybrid systems of immobilized photosensitizers on npAu by adjusting the spectral overlap integral between the plasmonic states of npAu and the excited states of the sensitizer in order to make energy transfer more efficient and energetically favourable.

Preparation and characterization of npAu foils functionalized with the ZnPc derivative

The functionalization of the as prepared npAu foils was achieved employing a two-step functionalization approach established in our group (Fig. 4).[24,25] In a first step, the npAu foil was functionalized using the principle of a SAM using **1** resulting in a system bearing free azide groups at the surface. Secondly, these azide groups were used to perform a CuAAC ("click reaction") to attach the peripherally alkyne-substituted ZnPc photosensitizer onto the npAu surface.

The advantage of the npAu foils over npAu disks and powders used in our previous studies is shown by the possibility

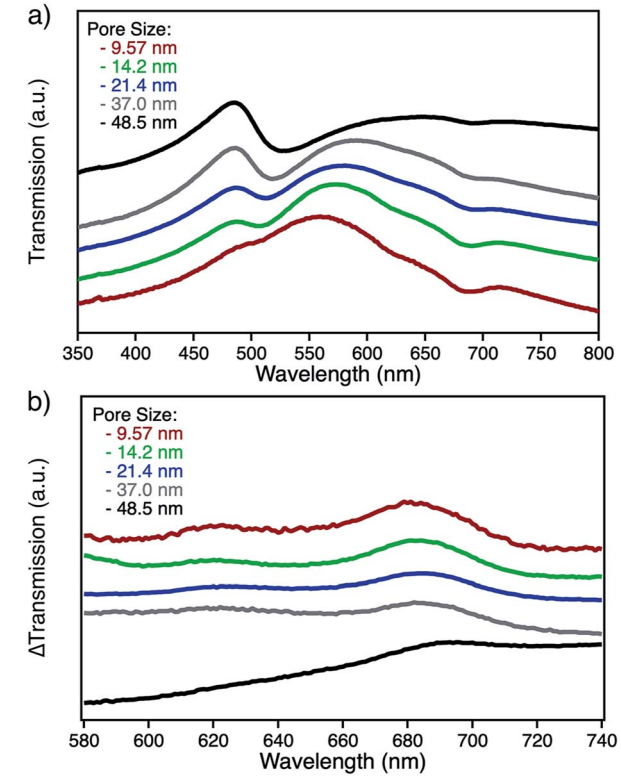

Fig. 5 (a) UV-Vis transmission spectra of ZnPc functionalized npAu foils in a DMF surrounding environment after dealloying times of 15 min (red), 30 min (green), 2 h (blue), 8 h (grey) and 72 h (black) and (b) Differential spectra of functionalized and unfunctionalized npAu foils showing the absorption of the immobilized ZnPc derivative **2**.

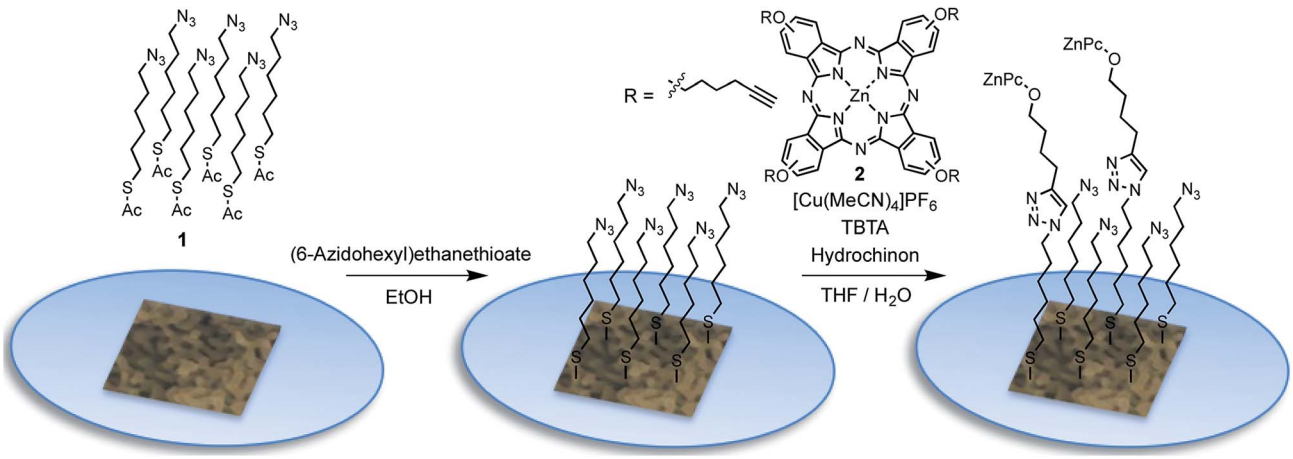

Fig. 4 Schematic representation of the functionalization of the npAu foils: formation of the azide terminated alkanethiol self-assembled monolayer (SAM) in the first step using *S*-(6-azidohexyl)ethanethioate (**1**) followed by copper catalyzed azide–alkyne cycloaddition (CuAAC, "click chemistry") to bind the alkyne-substituted ZnPc derivative **2**.

Table 1 Properties and photocatalytic activity of different npAu hybrids prepared by various free corrosion dealloying times. P_S – determined average pore sizes at the surface, L_S – determined average ligament sizes at the surface both obtained from SEM, $\lambda_{Longitudinal}$ – position of the longitudinal part of the plasmon resonance in the UV-Vis spectrum, $\lambda_{Transverse}$ – position of the transverse part of the plasmon resonance in the UV-Vis spectrum, $\chi_{Zn,\ EDX}$ immobilized Zn content given as weight% as obtained by EDX spectroscopy and conversion – maximum oxidation by sensitized $^1O_2$ after 20 min irradiation time

Dealloying (min)	P_S (nm)	L_S (nm)	S ($m^2\ g^{-1}$)	$\lambda_{Longitudinal}$ (nm)	$\lambda_{Transverse}$ (nm)	$\chi_{Zn,\ EDX}$ (wt%)	$Conversion_{DPBF}$ (%)
15	9.57 ± 1.79	11.11 ± 1.88	16.82	553	492	1.5	20.69
30	14.18 ± 2.39	15.08 ± 2.59	13.16	560	490	0.9	29.07
120	21.37 ± 3.42	21.08 ± 3.54	8.86	576	488	0.6	19.02
720	37.00 ± 7.47	39.16 ± 7.62	4.77	590	486	0.1	14.04
4320	48.46 ± 10.27	66.52 ± 12.68	2.81	643	485	Not detected	9.02

to directly provide evidence for the successful linkage of the macrocycle to the npAu by UV-Vis spectroscopy (Fig. 5a). As the samples were measured in transmission mode, the signals of the ZnPc appear as negative peaks in the spectra. Using the spectra of the unfunctionalized npAu supports (Fig. 3) it was possible to obtain differential spectra clearly showing the absorption of the immobilized ZnPc (Fig. 5b). The surface concentration of immobilized ZnPc shows a direct dependency on the pore size of the support. The reason for that is due to larger specific surface areas for npAu with smaller pores, which was calculated according to a literature method to range from 2 to 17 $m^2\ g^{-1}$, resulting in an increased available surface per support for the ZnPc immobilization.[40,41] For a more precise analysis, the samples were also studied by SEM and EDX measurements. The pore and ligament sizes were found to be unaffected by the organic functionalization and were the same as in the precursor supports, as already shown for npAu disks and powders.[25] EDX mapping on the surface of a modified npAu foil also confirmed a homogenous distribution of the photosensitizer over the entire surface (Fig. S3†). The trend of increasing ZnPc immobilization shown by UV-Vis spectroscopy was also confirmed by the EDX measurements (Table 1). For the EDX measurements it turned out to be crucial to transfer the hybrid foil samples from the supporting microscope cover glass directly onto the conducting carbon tape of the SEM sample holder, as the EDX measurement of a bare microscope cover slide showed the presence of around 5 at% of zinc contained in the glass. The absolute amount of immobilized ZnPc was too small for exact determination, as the values obtained from EDX spectroscopy are extremely close to the detection limit and are only good to support the observed trend already seen by UV-Vis spectroscopy. Therefore, the specific surface area for every hybrid system was calculated (Table 1) and used for comparison, assuming a weight of 0.05 mg for the npAu support for further discussion. A direct weighing of the samples was not possible as the samples were to light. We hence calculated the weight based on the specific density (50 wt%) of the Ag/Au starting alloy and its dimensions.

Photooxidation of DPBF by ZnPc functionalized npAu foils

As already mentioned in the previous sections, the resulting npAu foils all exhibit a thickness of only around 100 nm, as determined by SEM (Fig. S2†), resulting in a porous structure completely irradiated during the photooxidation experiments. In addition, having npAu foils with different pore sizes in hand, the hybrid photocatalysts can be tested regarding diffusion limitation phenomena. But, as summarized in Table 1, the

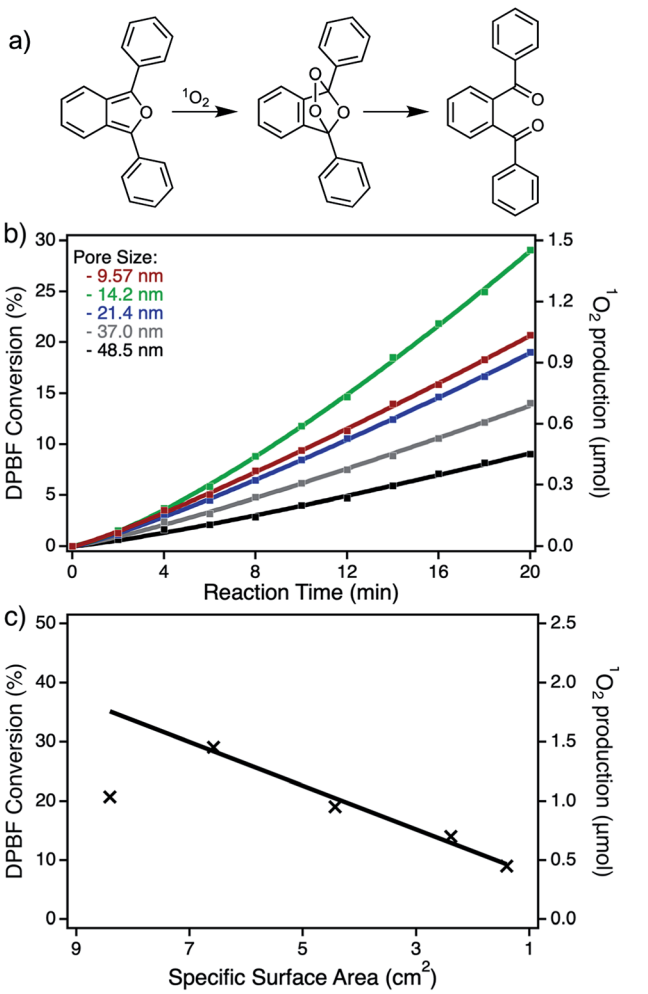

Fig. 6 (a) Reaction scheme for the photooxidation of DPBF by $^1O_2$. (b) Photocatalytic DPBF oxidation over time by npAu photocatalytic coatings with pore sizes of 9.57 nm (red), 14.2 nm (green), 21.4 nm (blue), 37.0 nm (grey) and 48.5 nm (black). (c) Plot of the maximum conversion after 20 min *vs.* the specific surface area of the corresponding hybrid for visualization of diffusion limitation and mass transport phenomena.

change in pore size is coherent with a change in the specific surface area, since smaller pore sizes result in a higher available surface area that has to be considered during the functionalization with the photosensitizer. The UV-Vis and EDX measurements both confirmed the expected increase in immobilized Zn content for the samples bearing smaller pores (Fig. 5b and Table 1).

The photocatalytic experiments clearly show this trend resulting in a higher DPBF conversion, based on a higher amount of sensitized singlet oxygen, with increasing ZnPc coverage (Fig. S4,† Fig. 6b). Assuming a constant immobilization fraction of the ZnPc, the increase in singlet oxygen sensitization should be proportional to the calculated specific surface area. The plot of the maximum DPBF conversion after an irradiation time of 20 min against the specific surface area of the used hybrid material shows the linear dependency of the activity to the surface area for all samples with pore sizes between 14 and 50 nm. Only the sample with a pore size below 14 nm shows a significant deviation from this trend, which is ascribed to the diffusion limitation at small pore sizes. Except for this one particular sample, no limitation by diffusion was observed (Fig. 6c). In addition, the effect of higher ZnPc immobilization completely dominates any effect of plasmonic shift that should contrarily increase the activity for samples with larger pores and therefore smaller surface areas. Transferring those results to the hybrid systems based on npAu powder described in our previous study, the reduction of the pore sizes to 15 nm could be a promising strategy for optimization of the overall activity.[25] Those powder hybrid systems seem to be the best solution for batch reactors, whereas the npAu foils represent a promising material used as catalytic coatings in flow reactors, making them also an interesting material for industrial applications.

Conclusions

This study is, best to our knowledge, the first example of npAu foils functionalized with a photosensitizer and the usage of those new hybrid materials as photocatalytic coatings for singlet oxygen sensitization. Hybrid materials were prepared on npAu foils with pore sizes between 9–50 nm and an increasing amount of immobilized photosensitizer was found in both, UV-Vis and EDX spectroscopic measurements for npAu supports with smaller pore sizes and accordingly larger specific surface areas. The photocatalytic activity of singlet oxygen sensitization was shown to be exclusively dominated by the amount of immobilized sensitizer suppressing every indication of changing interaction due to the shift of the corresponding surface plasmon resonance of npAu with altering pore size. In addition, the photocatalytic results clearly confirm that mass transport and diffusion limitation are becoming predominant for the sample with pore sizes below 14 nm. Thus, the hybrid material on a npAu support with defined pore sizes of around 15 nm shows the highest singlet oxygen sensitization activity due to the largest specific surface area and maximum sensitizer coverage above the diffusion limited regime.

Conflicts of interest

There are no conflicts of interest to declare.

Acknowledgements

We gratefully acknowledge the experimental support of Petra Witte (Department of Historic Geology and Paleontology, University of Bremen, Bremen, Germany) during the SEM and EDX measurements as well as the lab technician trainees Rebecca Siemering, Jasmin Richter and Rieke Norden for their contribution within the synthesis of compounds **1** and **2**. We also acknowledge the discussion of the manuscript with Prof. Marcus Bäumer (Institute of Applied and Physical Chemistry, University of Bremen, Bremen, Germany). The project was funded by Deutsche Forschungsgemeinschaft (DFG) within the grants WI 4497/3-1 and WO 237/42-1.

References

1 P. N. Ciesielski, A. M. Scott, C. J. Faulkner, B. J. Berron, D. E. Cliffel and G. K. Jennings, *ACS Nano*, 2008, **2**, 2465–2472.
2 F. Jia, C. Yu, Z. Ai and L. Zhang, *Chem. Mater.*, 2007, **19**, 3648–3653.
3 X. Ge, R. Wang, P. Liu and Y. Ding, *Chem. Mater.*, 2007, **19**, 5827–5829.
4 Z. Liu and P. C. Searson, *J. Phys. Chem. B*, 2006, **110**, 4318–4322.
5 F. Jia, C. Yu, K. Deng and L. Zhang, *J. Phys. Chem. C*, 2007, **111**, 8424–8431.
6 J. Zhang, P. Liu, H. Ma and Y. Ding, *J. Phys. Chem. C*, 2007, **111**, 10382–10388.
7 V. Zielasek, B. Jürgens, C. Schulz, J. Biener, M. M. Biener, A. V. Hamza and M. Bäumer, *Angew. Chem., Int. Ed.*, 2006, **45**, 8241–8244.
8 R. Zeis, T. Lei, K. Sieradzki, J. Snyder and J. Erlebacher, *J. Catal.*, 2008, **253**, 132–138.
9 C. Xu, X. Xu, J. Su and Y. Ding, *J. Catal.*, 2007, **252**, 243–248.
10 R. Zeis, A. Mathur, G. Fritz, J. Lee and J. Erlebacher, *J. Power Sources*, 2007, **165**, 65–72.
11 J. Erlebacher, M. J. Aziz, A. Karma, N. Dimitrov and K. Sieradzki, *Nature*, 2001, **410**, 450.
12 A. Wittstock, J. Biener, J. Erlebacher and M. Bäumer, *Nanoporous Gold: From an Ancient Technology to a High-Tech Material*, RSC Publishing, RSC Nanoscience and Nanotechnology, 2012.
13 A. Wittstock, A. Wichmann and M. Bäumer, *ACS Catal.*, 2012, **2**, 2199–2215.
14 A. Wittstock, A. Wichmann, J. Biener and M. Bäumer, *Faraday Discuss.*, 2011, **152**, 87–98.
15 J. Shi, C. Mahr, M. M. Murshed, T. M. Gesing, A. Rosenauer, M. Baumer and A. Wittstock, *Phys. Chem. Chem. Phys.*, 2017, **19**, 8880–8888.
16 A. Lackmann, C. Mahr, M. Schowalter, L. Fitzek, J. Weissmüller, A. Rosenauer and A. Wittstock, *J. Catal.*, 2017, **353**, 99–106.

17 A. Lackmann, C. Mahr, A. Rosenauer, M. Bäumer and A. Wittstock, *Catalysts*, 2019, **9**, 416.
18 G. Pattrick, E. van der Lingen, C. W. Corti, R. J. Holliday and D. T. Thompson, *Top. Catal.*, 2004, **30**, 273–279.
19 X. Lang, L. Quian, P. Guan, J. Zi and M. Chen, *Appl. Phys. Lett.*, 2011, **98**, 093701.
20 F. Zhao, J. Zeng and W.-C. Shih, *Sensors*, 2017, **17**, 1519.
21 E. Detsi, M. Salverda, P. R. Onck and J. T. M. De Hosson, *J. Appl. Phys.*, 2014, **115**, 044308.
22 A. Wichmann, A. Wittstock, K. Frank, M. Biener Monika, B. Neumann, L. Mädler, J. Biener, A. Rosenauer and M. Bäumer, *ChemCatChem*, 2013, **5**, 2037–2043.
23 J. Shi, C. Mahr, M. M. Murshed, V. Zielasek, A. Rosenauer, T. M. Gesing, M. Baumer and A. Wittstock, *Catal. Sci. Technol.*, 2016, **6**, 5311–5319.
24 A. Wichmann, G. Schnurpfeil, J. Backenköhler, L. Kolke, V. A. Azov, D. Wöhrle, M. Bäumer and A. Wittstock, *Tetrahedron*, 2014, **70**, 6127–6133.
25 D. Steinebrunner, G. Schnurpfeil, A. Wichmann, D. Wöhrle and A. Wittstock, *Catalysts*, 2019, **9**, 555.
26 A. Kotiaho, R. Lahtinen and H. Lemmetyinen, *Pure Appl. Chem.*, 2011, **83**, 813.
27 A. Kotiaho, R. Lahtinen, A. Efimov, H.-K. Metsberg, E. Sariola, H. Lehtivuori, N. V. Tkachenko and H. Lemmetyinen, *J. Phys. Chem. C*, 2010, **114**, 162–168.
28 S. Moeno, E. Antunes and T. Nyokong, *J. Photochem. Photobiol., A*, 2011, **222**, 343–350.
29 N. Masilela, E. Antunes and T. Nyokong, *J. Porphyrins Phthalocyanines*, 2013, **17**, 417–430.
30 A. R. Karimi, A. Khodadadi and M. Hadizadeh, *RSC Adv.*, 2016, **6**, 91445–91452.
31 Y. Ding, Y.-J. Kim and J. Erlebacher, *Adv. Mater.*, 2004, **16**, 1897–1900.
32 T. Förster, *Ann. Phys.*, 1948, **437**, 55–75.
33 G. C. Bazan, *J. Org. Chem.*, 2007, **72**, 8615–8635.
34 L. Yuan, W. Lin, K. Zheng and S. Zhu, *Acc. Chem. Res.*, 2013, **46**, 1462–1473.
35 S.-M. Chang, Z. Tu, H.-M. Jan, J.-F. Pan and C.-H. Lin, *Chem. Commun.*, 2013, **49**, 4265–4267.
36 Q. H. Sodji, V. Patil, J. R. Kornacki, M. Mrksich and A. K. Oyelere, *J. Med. Chem.*, 2013, **56**, 9969–9981.
37 C. Ligeour, A. Meyer, J.-J. Vasseur and F. Morvan, *Eur. J. Org. Chem.*, 2012, **2012**, 1851–1856.
38 T. R. Chan, R. Hilgraf, K. B. Sharpless and V. V. Fokin, *Org. Lett.*, 2004, **6**, 2853–2855.
39 C. J. Brassard, X. Zhang, C. R. Brewer, P. Liu, R. J. Clark and L. Zhu, *J. Org. Chem.*, 2016, **81**, 12091–12105.
40 Y. H. Tan, J. A. Davis, K. Fujikawa, N. V. Ganesh, A. V. Demchenko and K. J. Stine, *J. Mater. Chem.*, 2012, **22**, 6733–6745.
41 E. Detsi, E. De Jong, A. Zinchenko, Z. Vuković, I. Vuković, S. Punzhin, K. Loos, G. ten Brinke, H. A. De Raedt, P. R. Onck and J. T. M. De Hosson, *Acta Mater.*, 2011, **59**, 7488–7497.
42 W. Spiller, H. Kliesch, D. Wöhrle, S. Hackbarth, B. Röder and G. Schnurpfeil, *J. Porphyrins Phthalocyanines*, 1999, **2**, 145–158.
43 E. Lemp, C. Valencia and A. L. Zanocco, *J. Photochem. Photobiol., A*, 2004, **168**, 91–96.
44 T. Sato, Y. Hamada, M. Sumikawa, S. Araki and H. Yamamoto, *Ind. Eng. Chem. Res.*, 2014, **53**, 19331–19337.